Clays and Clay Minerals, Vol. 60, No. 3, 254–264, 2012.

SYNTHESIS AND PROPERTIES OF Sn-CONTAINING MAGADIITE

Wojciech Supronowicz[1,*], Frank Roessner[1], Wilhelm Schwieger[2], Mikhail Meilikhov[3], and Daniel Esken[3]

[1] Carl von Ossietzky University, Faculty of Natural Sciences, Industrial Chemistry II, D-26-111 Oldenburg, Germany
[2] Lehrstuhl für Chemische Reaktionstechnik Friedrich-Alexander-Universität Erlangen-Nürnberg, Egerlandstrasse 3, D-91-058 Erlangen, Germany
[3] Lehrstuhl für Anorganische Chemie II NC 2, Universitaetstrasse 150 D-44-801 Bochum, Germany

Abstract—Hydrothermal syntheses of the magadiite, a layered silicate structure, were conducted in the presence of a heteroatom source ($SnCl_45H_2O$) with the intention of investigating its influence on the resulting material, as well as the possibility of isomorphous replacement of Si by Sn atoms in the above-mentioned structure. For comparison, unmodified magadiite, Al-containing magadiite, and impregnated magadiite were synthesized. The magadiite structure was identified for samples with Sn/Si ratios up to 0.015. Synthetic methods applied to Sn-modified materials were found to be unsuitable for the introduction of Al. The characterization methods used were X-ray diffraction, temperature-programmed reduction, and ^{29}Si magic angle spinning nuclear magnetic resonance and these revealed the substitution of Si by Sn in the silica layers. No additional acid centers on the surfaces of the modified samples were detected, suggesting the presence of the desired four-coordinate Sn in the silica layers.

Key Words—H_2-TPR, Magadiite, ^{29}Si MAS NMR, Textural Properties, Tin Silicate, XRD.

INTRODUCTION

The introduction of heteroatom tetrahedra into Si-based porous materials changes significantly the properties of the resulting material. Atoms such as Al, Ti, and Sn (referred to here as heteroatoms) generate additional isolated acid/basic sites, or redox active sites, which enhance the activity of porous material in various reactions. The modified material still has drawbacks relating to its original structures, unchanged after isomorphous substitution. An example of such a situation is titanosilicalite (TS-1). Although it is active in mild oxidation reactions (Wróblewska *et al*., 2006), its small pore radii limit significantly its application in the oxidation of bulky organic compounds. A material similar to three-dimensional silicates, capable of undergoing similar modifications (ion-exchange and isomorphous substitution) and with bigger pores than those of zeolites is needed.

Layered silicates consist of Si tetrahedra and hydrated cation layers. The distance between the silica layers can be adjusted, thereby enabling bulky organic molecules to access the eventual active centers located in or between the layers. The above-mentioned property gives layered silicates significant advantage over the microporous three-dimensional structure of zeolites. As for zeolites, the properties of layered silicates can be adjusted relatively easily by ion-exchange processes.

After exchange of interlayer Na^+ cations in various layered clay materials (*e.g.* ilerite, magadiite, and montmorillonite) with oxides or complexes containing species such as Pd, Ta, Nb, Pt, Ag, or Fe (Kim *et al.*, 2001, 2004; Kuhlmann *et al.*, 2004; Wang *et al.*, 2007; Yu and Yang, 2010; Schwieger *et al.*, 2003; Ozawa *et al.*, 2007), active catalysts were obtained for reactions such as the vapor-phase Beckmann rearrangement of cyclohexanone oxime (Kim *et al.*, 2001, 2004) and conversion of *n*-hexane (Wang *et al.*, 2007). Organic compounds, even the bulky ones, can also be introduced (Peng *et al*., 2006). After organosilylation, layered silicates can also be used as adsorbents (Sprung *et al*., 1990; Royer *et al*., 2010).

Ion exchange has been useful in the synthesis of various porous materials. For example, the synthesis of silica-1 and silica-2 was possible (Feng *et* al., 2004; Kiyozumi *et* al., 1998; Kiyozumi *et* al., 2002) after the introduction of templates into the interlayer space. Successful synthesis of magadiite-based mesoporous composites has also been reported (Fudala *et al*., 2000). Moreover, the first mesoporous silica material, FSM-16, was prepared from kanemite intercalated with hexadecyltrimethylammonium cations (Yanagisawa *et al*, 1990).

Modified layered silicates were also used as precursors of Al-containing microporous materials. An ion-exchange process was used to introduce Al-containing compounds and templates into the interlayer space with the intention of obtaining a porous precursor material (Selvam *et al*., 2003). The modification method mentioned was not the only one which was used to introduce Al into the material. Isomorphic replacement of Si atoms within the silicate layers with Al and B atoms was demonstrated by Pál-Borbély *et al.* (1997, 1998), Superti *et al.* (2007), and Mihályi *et al.* (2007). The approach is

* E-mail address of corresponding author:
wojciech_supronowicz@o2.pl
DOI: 10.1346/CCMN.2012.0600303

similar to that used for zeolites, where active transition metals such as Ti or Fe have been introduced.

Based on numerous reports (Azizi and Yousefpour, 2011; Corma *et al*., 2003; Lazar *et al*., 2000; Renz *et al*., 2002; Szostak *et al*., 1987) of the successful incorporation of various heteroatoms into zeolite frameworks, similar modification of layered silicates are assumed to be possible also. Substitution of Si atoms in layered silicates by transition metals could result in materials capable of mild oxidation reactions. Moreover, after the successful modification, the radius of pores could be adjusted by the introduction of different sized pillars between the silicate layers.

Based on the reports of Corma *et al.* (2003) and Boronat *et al*. (2007), who successfully introduced Sn into a zeolite structure and confirmed promotion of several reactions, *e.g.* the Meervein-Pendorv-Verley reduction and Baeyer-Villiger oxidation, Sn was chosen as the heteroatom.

The presence of a heteroatom source ($SnCl_4 \cdot 5H_2O$) in the ilerite synthesis mixture redirects the synthesis to the magadiite structure (Supronowicz and Roessner, 2011). The magadiite structure consists of silicate layers that are significantly thicker than those of ilerite (Figure 1) (Almond *et al*., 1997). The aim of the present work was to investigate the influence of a heteroatom source (especially $SnCl_4 \cdot 5H_2O$) on the synthesis of layered silicate-magadiite and to characterize the properties of the resulting material. In order to compare the properties of the synthesized materials with those already described in the literature (Pál-Borbély *et al.* 1997, 1998; Superti *et al.*, 2007; Mihályi *et al.*, 2007), a few samples were synthesized in which Si was partially substituted for Al.

EXPERIMENTAL

Unmodified magadiite, as well as samples with different Sn and Al contents, were synthesized according to the procedure proposed by Wang *et al.* (2006) (Figure 2). The chemical composition of the ideal unit cell of magadiite is $xM{:}Na_2O{:}(14-x)SiO_2{:}9H_2O$ (Wang *et al*., 2006), where *M* represents Al or Sn, and $0 \leqslant x \leqslant 1$. In standard synthesis, colloidal silica (CWK Bad Koestritz, Germany) was mixed with a heteroatom source, Sn(IV) chloride pentahydrate (Riedel-de Haen) or Al isopropoxide (Fluka), and dissolved in water. Then, NaOH (Merck) and Na_2CO_3 (Riedel-de Haen) were added in small amounts. A dense gel formed immediately after mixing all substrates (pH $\approx$ 12.5). The sample was then stirred vigorously for 1 h and sealed in a teflon-lined stainless steel autoclave. The molar ratios of the reactants in the synthesis mixture were $x{*}M{:}7SiO_2{:}(y{*}x{+}0.33)NaOH{:}0.66Na_2CO_3{:}100H_2O$, where y = 4 or 6 for the Al- or the Sn-samples, respectively. Crystallization took place at autogenous pressure at T = 423 K for 48 h under static conditions. Afterward, solid samples were washed and dried at 353 K. The resulting samples were named according to the ratio of heteroatom to Si atoms in a synthesis mixture: *xM*/7Si, where *M* = Sn or Al and *x* = molar ratio of *M*.

As has been reported by various authors, magadiite synthesis can be enhanced by the addition of Na carbonate as a co-source of Na (Fletcher and Bibby, 1987). Possible precipitation of Al(III)- or Sn(IV)-carbonate salts could occur during the synthesis. In order to determine the influence of the carbonate ions on the number of heteroatoms introduced and on the crystallinity of the resulting samples, syntheses with NaOH as the only source of Na were also carried out.

The influence of crystallization time on the synthesis was determined by prolonging it from 48 h to 72 h.

Syntheses with the addition of 0.1 g of the magadiite seeds were performed in an attempt to enhance the synthesis yield. Seeds were taken from the Na-magadiite sample.

In order to obtain supported bulky $Sn(IV)O_2$ (decoded as SnO_2/Na-magadiite), Na-magadiite was impregnated with Sn(IV)Cl. The ratio of Sn (from the added salt) to Si was adjusted to represent the Sn/Si ratio found in the synthesis mixture of the Sn-substituted

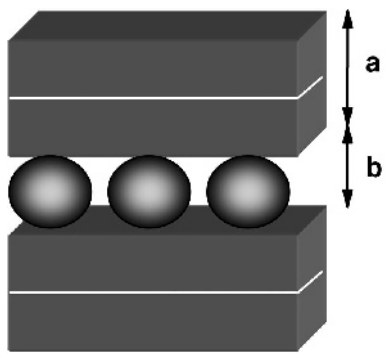

Figure 1. Magadiite structure: (a) two layers of tetrahedrally coordinated Si; (b) hydrated cation layer.

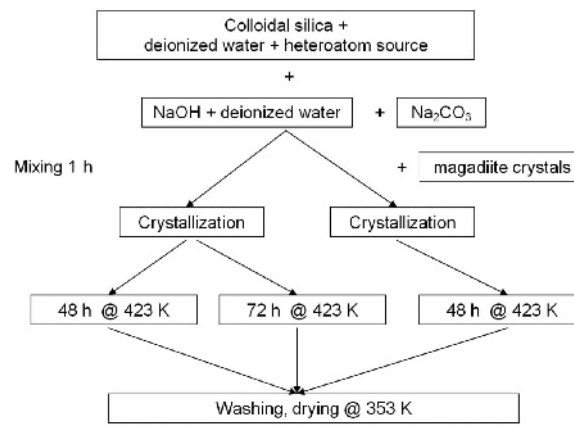

Figure 2. Synthesis procedures applied.

https://doi.org/10.1346/CCMN.2012.0600303 Published online by Cambridge University Press

magadiite samples with the greatest Sn content. After mixing, the samples were heated to 383 K.

The H forms of the samples were obtained after dispersing 2 g of a Na-sample in 40 mL of deionized water. The pH was adjusted to 2 by adding 0.1 M HCl. After 24 h of stirring, the H form of the material was washed, filtered, and dried at 353 K.

X-ray diffraction (XRD) patterns were recorded using a Stoe STADI P instrument (Darmstadt, Germany). The measurements at low-angle diffraction were made using a Philips X'Pert (Almelo, The Netherlands).

Scanning electron microscopy (SEM) micrographs were obtained using an FEI QUANTA 200 3D instrument (Eindhoven, The Netherlands).

The N_2 adsorption isotherms were determined on an Autosorb-1 Quantachrome at T = 77 K. Prior to adsorption, samples were evacuated at 573 K. The BET method was used to determine the surface area.

Inductively coupled plasma atomic emission spectroscopy (ICP-AES) analysis was carried out using a Thermo Scientific iCAP 6000 series and conducted after dissolving 100 mg of sample in 500 mg of 48% HF solution. The above-mentioned amount of acid was used to ensure complete dissolution of the sample.

In differential thermal analysis and thermal gravimetry analysis (DTA/TG) (TGA/SDTA 851^e-Mettler-Toledo GMBH), samples were heated to 1273 K (heating rate: 10 K/min) in N_2 flow.

The acidity and reducibility of the samples were determined using a modified AMI-100 unit (Raczek Analysentechnik, Garbsen, Germany). In the temperature-programmed ammonia desorption (NH_3-TPD) tests, 0.3 g of a sample (200–315 μm grainsize fraction) was heated in He (50 mL/min) up to 573 K at a heating rate of 20 K/min. Then the samples were treated with He containing 5% NH_3 (25 mL/min) at 343 K for 30 min. The physically adsorbed NH_3 was removed at 423 K in He (50 mL/min) over 2 h. Desorption of the chemisorbed NH_3 was conducted in He (50 mL/min) in the temperature range 423–973 K with the heating rate 10 K/min. The amount of NH_3 desorbed was recorded using a thermal conductivity (TCD) detector.

In hydrogen temperature-programmed reduction (H_2-TPR), 0.3 g of sample (315–200 μm grain-size fraction) was placed in a quartz u-pipe. During the pretreatment procedure the sample was heated in an Ar stream (50 mL/min) to 573 K at a heating rate of 20 K/min. After 2 h the sample was cooled to 373 K. The reduction measurement was conducted under a flow of Ar (50 mL/min), containing 7.5% H_2, by heating the samples to 973 K (5 K/min). Hydrogen consumption was detected by a TCD detector.

Diffuse reflectance infrared Fourier transform (DRIFT) spectra were recorded using a Bruker EQUINOX 55 instrument equipped with a Diffuse Reflection Attachment and a Harricks high-temperature dome at 373 K under constant N_2 flow (50 mL/min). The samples were diluted with diamond powder (1:4) to improve the reflection at low wavenumbers.

Solid-state nuclear magnetic resonance (NMR) spectra were measured using a Bruker DSX 400 MHz instrument under magic-angle spinning (MAS) conditions in 2.5 mm ZrO_2 rotors with a sample volume of 12 μL (rotation frequency 20 kHz). The ^{29}Si-CP-NMR (79.460 MHz) was carried out with the pulse program CP4C and tetramethylsilane (TMS) as the reference.

The conversion of 2-methyl-3-butyn-2-ol (MBOH) (Lancaster) mixed with toluene as an internal standard (Fluka) was carried out in a fixed-bed reactor, embedded in a computer-controlled bench unit. In order to provide a steady feed rate (0.02 mL/min) to the reactor, the reaction mixture (95 vol.% of MBOH and 5 vol.% toluene) was held in a vessel at constant temperature (287 K) and N_2 was passed through it. Samples (0.2 g of

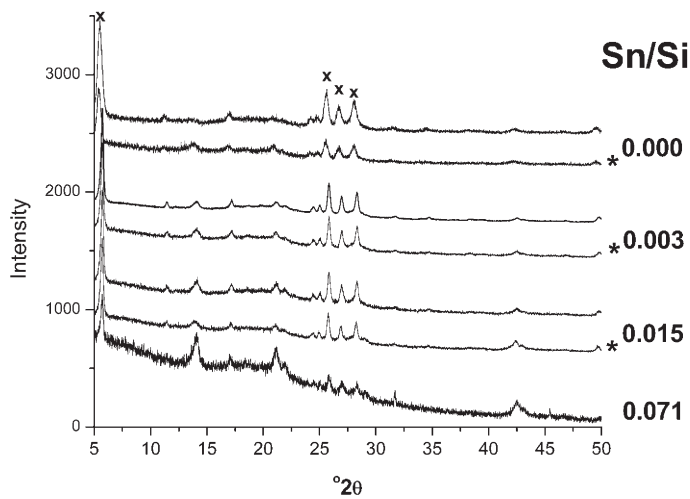

Figure 3. XRD patterns of samples with different Sn loadings. * Synthesis without Na_2CO_3. x: typical reflections of the magadiite structure.

https://doi.org/10.1346/CCMN.2012.0600303 Published online by Cambridge University Press

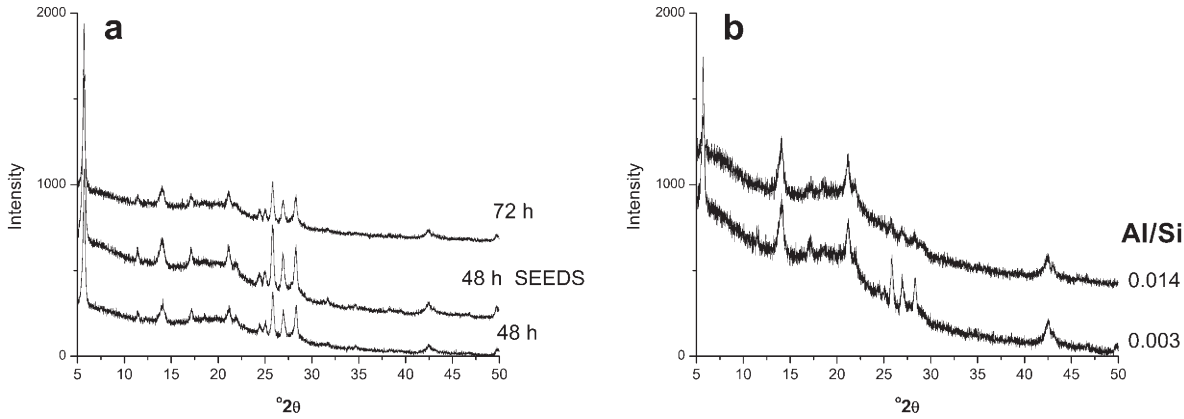

Figure 4. (a) XRD profiles of 0.015 Sn/Si samples synthesized over different time periods and in the presence of magadiite seeds; (b) XRD profiles of various Al-containing samples.

the 200–315 μm grain-size fraction) were placed in the center of the tubular reactor. Samples were activated at 773 K in air, which was subsequently replaced by N_2, which was then passed through the catalyst bed for 4 h. The reaction was carried out at 393 K. The reaction products were analyzed on-line using a gas chromatograph (HP 5890 Series II) equipped with a capillary column (OPTIMA-WAX – 0.25 μm; 60 m × 0.25 mm) and a flame ionization detector (FID).

RESULTS AND DISCUSSION

The XRD patterns of the synthesized samples (Figures 3–5) revealed that both synthesis routes (with or without CO_3^{2-} anions) led to the magadiite structure (typical 2θ values of ~5.6º, 25.8º, 26.9º, 28.3º) (Pál-Borbély *et al*., 1998, Feng and Balkus, 2003). Furthermore, the addition of carbonate anions to the synthesis mixture had a moderate influence on the crystallinity. On the other hand, the crystallinity decreased with increasing Sn content. Samples with the highest Sn loading (0.071 Sn/Si – Figure 3) contained only traces of the magadiite phase. Different synthesis procedures had no significant influence on the crystallinity (Figure 4a).

Only traces of the magadiite phase were found in Al-containing samples (Figure 4b) with Al/Si ⩾ 0.015, which is a far smaller value than that in the case of Sn-containing magadiite. A similar relation was reported for modified ilerite synthesis (Supronowicz and Roessner, 2011). The presence of the Al heteroatom in the applied synthesis conditions is, therefore, suspected of directing the synthesis toward an amorphous material. One should note that the Al-containing samples were synthesized only for comparison reasons. The syntheses were not optimized in order to obtain high Al loading; therefore, the Al content in the samples was smaller than that reported by other authors (Superti *et al.*, 2007).

All of the modified samples contained impurities of amorphous material and quartz (see also the next paragraph). A similar position for the basal spacing peak (5.6º2θ) for different samples (Figure 5) indicated the same distance between the layers and the lack of pillars between them.

All magadiite samples consisted of agglomerates of rosette-shaped crystals (Figure 6), the shape of which was typical of the crystal structure for that phase (Iwasaki *et al*., 2006). The SEM images indicated the presence of an amorphous material on the surface of the Sn-containing samples (Figure 6c–e), which correlated well with the XRD results (Figures 3, 4). Samples synthesized without Na_2CO_3 had slightly different topographies, *i.e.* flatter crystals than those synthesized with it. Crystals of the modified samples synthesized without Na_2CO_3 were slightly larger (Figure 6c,d). A decrease in the crystal size was also observed in the case of the sample synthesized in the presence of the magadiite seeds (Figure 6e).

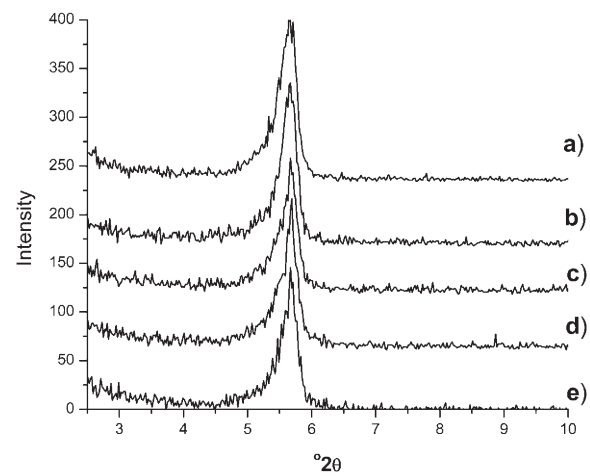

Figure 5. Basal spacing reflections of various samples: (a) 0.000 Sn/Si synthesized with Na_2CO_3; (b) 0.015 Sn/Si synthesized without Na_2CO_3; (c) 0.015 Sn/Si synthesized with Na_2CO_3; (d) 0.015 Sn/Si synthesized with Na_2CO_3 in 72 h; (e) 0.015 Sn/Si synthesized with Na_2CO_3 with magadiite seeds.

https://doi.org/10.1346/CCMN.2012.0600303 Published online by Cambridge University Press

Table 1. Sn/Si ratio of the synthesis mixtures and Sn content in the bulk solid, determined by ICP-AES.

Sn/Si in synthesis mixture	Synthesis mixture	Sn/Si in sample
0.007	Standard	0.0093
0.015	Standard	0.0198
0.015	Without Na_2CO_3	0.0183
0.015	3 days of synthesis	0.0189
0.015	Synthesis in the presence of magadiite seeds	0.1916

The Sn content in various samples was analyzed by ICP-AES elemental analysis and reported as the ratio of the sum of all kinds of Sn present in the material to Si (Table 1). Modification of the synthesis route (use of magadiite seeds, change of synthesis time, *etc*.) had no noticeable effect on the Sn/Si ratio in the samples (Table 1). For all samples, the measured Sn/Si ratio was significantly greater than in the synthesis mixture. This can be explained by assuming that not all the Si was used during the synthesis to build the layered structure, *i.e.* a noticeable amount of Si remained in the synthesis liquor.

In order to establish the thermal properties of the samples obtained, the DTA/TG studies were carried out. The DTA pattern for as-synthesized magadiite (Figure 7a,b) corresponded well to those described in the literature (Schwieger *et al*., 2003). Endothermic maxima at ~370 K and 450 K (Figure 10) were attributed to desorption of water from the interlayer space and to destruction of the hydration shell of the interlayer Na cations, respectively. Note that for the H-magadiite, the above-mentioned peaks were not observed due to the lower basal spacing of such material (Lagaly *et al*., 1975; Macedo and Airoldi, 2006). Recorded profiles of the modified samples were identical to those of Na-magadiite and so clearly neither the amount of Sn introduced nor the synthesis route had any influence on the thermal properties of the samples.

The presence of only one peak arising from the desorption of physisorbed water in the DTA profile of the H form of the modified samples (Figure 7b) indicated that the exchange of Na by protons was probably nearly complete.

The surface area did not change significantly with increasing Sn content (Table 2). The adsorption isotherm (Figure 8) confirmed the absence of micropores and the presence of meso- and macropores (Macedo and Airoldi, 2006). After considering the XRD patterns (Figure 5), the above-mentioned pores can be considered to be present between the crystals in agglomerates, as well as in the amorphous material present in the samples (as confirmed by the SEM images). Isotherms of other samples were similar (data not shown), and so the lack of significant changes in the surface area and the lack of indication of the presence of micropores suggested the absence of interlayer pillars (particularly those due to Sn oxide species).

The infrared (IR) spectra in the lattice vibration range (Figure 9) revealed that the spectra of the Na-magadiite are similar to those described in the literature (Borbely *et al*., 1991; Kim *et al*., 2004). According to various authors (Borbely *et al*., 1991; Kim *et al*., 2004; Li *et al*., 2010), *Me*−O−Si vibrations (where *Me* = metal) are characterized by a band at ~970 cm^{-1}. The band is suggested to indicate the presence of *Me* in the layer, as well as bonding between the interlayer metallic oxide and the silicate layer (Szostak *et al*., 1987). All of the heteroatom-containing samples synthesized exhibited a broadening of the band from asymmetric vibrations of Si−O−Si (970−1100 cm^{-1}), which may indicate the presence of an Si−O−Sn bond in the silicate layers (Yu and Yang, 2010; Khouw and Davis, 1995; Macedo and Airoldi, 2006); such a conclusion appears to be speculative because the DRIFT technique is relatively difficult to quantify. Moreover, the above-mentioned band can also be ascribed to Si−O−H bending vibrations (Camblor *et al*., 1993).

In order to assess the chemical environment around the Si atoms in the framework, selected samples were studied by means of ^{29}Si magic-angle spinning nuclear magnetic resonance (MAS NMR) spectroscopy: spectra of the Na-magadiite sample showed signals at −101 and −104 ppm (Figure 10a) which can be assigned to the $Si(OSi)_4$ silicate species (Q_4 signal) (Macedo and Airoldi, 2006). The Q_4 signal split was suggested by

Table 2. Texture data for various samples synthesized with Na_2CO_3.

Sn/Si	Surface area (m^2/g)
0.000 Sn/Si	97
0.007 Sn/Si	88
0.015 Sn/Si	79
0.015 Sn/Si*	80
0.015 Sn/Si†	83
SnO_2/Na-magadiite	75
Al/Si	
0.003 Al/Si	88

* 72 h of synthesis
† Synthesis in the presence of magadiite seeds

https://doi.org/10.1346/CCMN.2012.0600303 Published online by Cambridge University Press

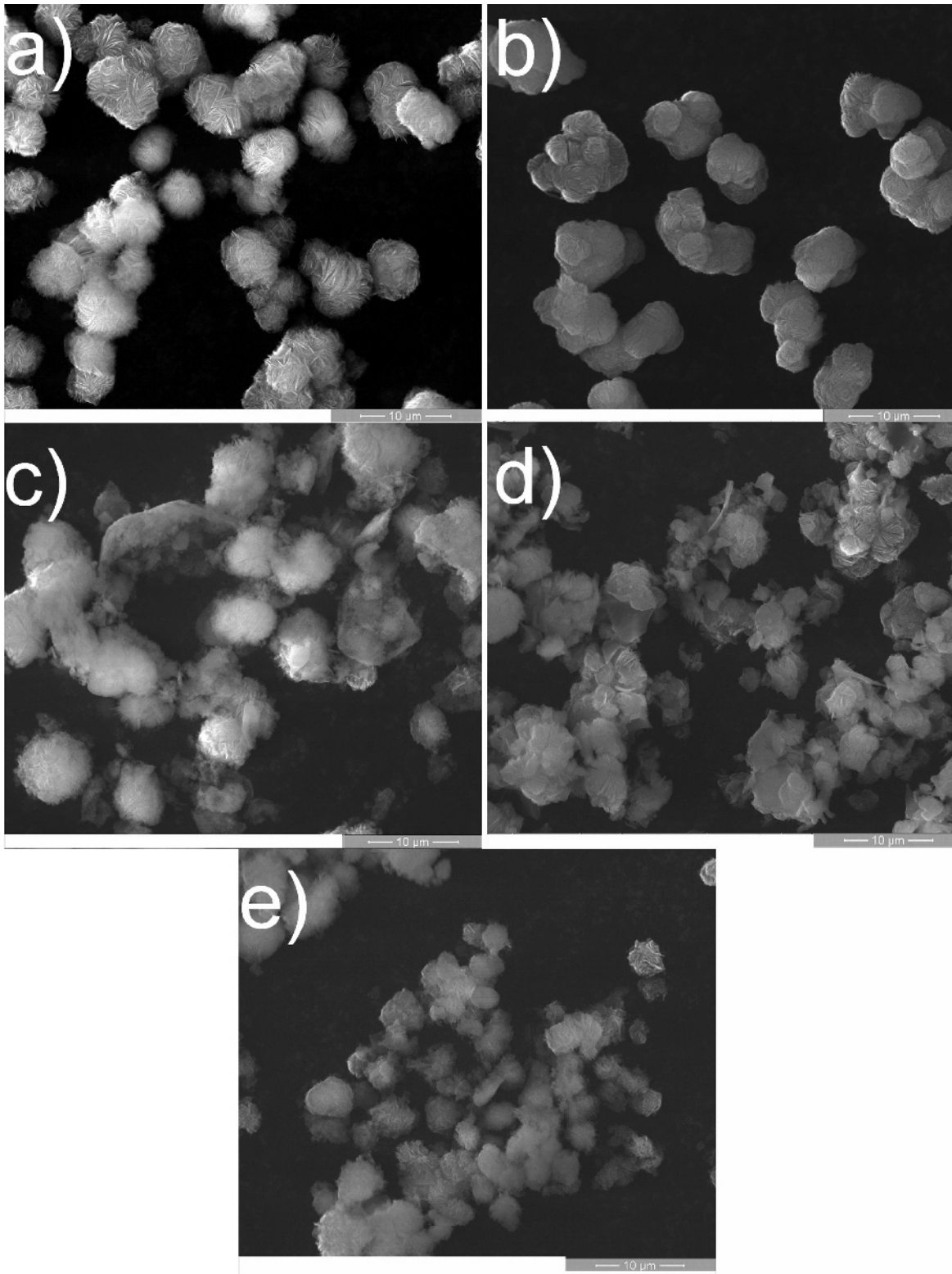

Figure 6. SEM images of various samples: (a) 0.000 Sn/Si synthesized with Na_2CO_3; (b) 0.000 Sn/Si synthesized without Na_2CO_3; (c) 0.015 Sn/Si synthesized with Na_2CO_3; (d) 0.015 Sn/Si synthesized without Na_2CO_3; (e) 0.015 Sn/Si synthesized with Na_2CO_3 and magadiite seeds.

https://doi.org/10.1346/CCMN.2012.0600303 Published online by Cambridge University Press

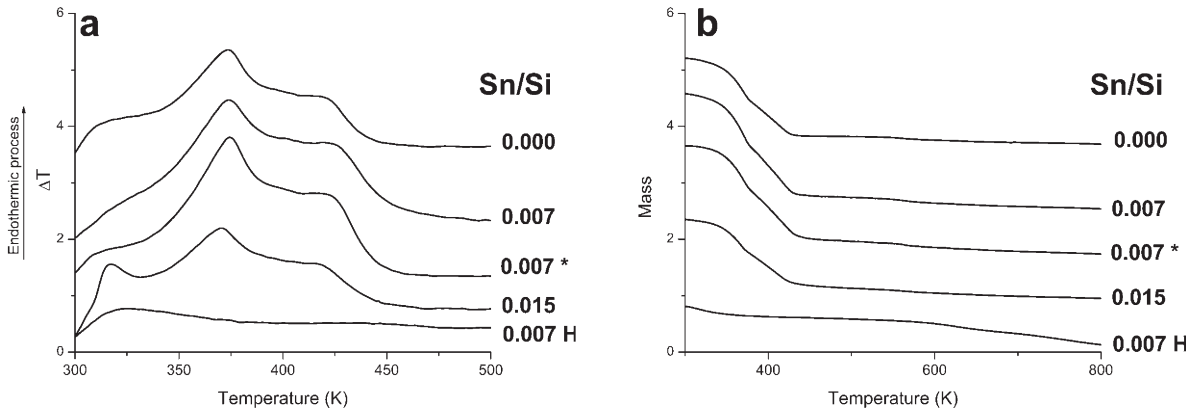

Figure 7. DTA (a) and TG (b) profiles of different Na samples. H – H form of the sample; * synthesis without Na_2CO_3.

Almond *et al.* (1997) to be caused by the differences between $Si(OSi)_4$ (*e.g.* in average Si–O–Si bond angles) which make up the magadiite layer. In addition, an intense signal at ~–89 ppm was noticed. This was assigned to the HO–$Si(OSi)_3$ silicate species (Q_3 signal) (Macedo and Airoldi, 2006). As can be seen in the example of the 0.015 Sn/Si sample synthesized in the presence of carbonate anions (Figure 10b), the Q_3 signal was much more intense, probably due to larger amounts of amorphous material present in the sample. A split of the above-mentioned Q_3 signal was also noticed. An assumption can be made that the split was caused by *R*–O–$Si(OSi)_3$, where *R* = Sn or H. However, the published data do not provide an unequivocal interpretation of the spectra (Renz *et al.*, 2002).

The redox properties of the modified samples were investigated by H_2-TPR (Figure 11). Bulky SnO_2, SnO_2/Na-magadiite, and Na-magadiite were also studied. Bulky SnO_2 was reduced in a single step at a temperature of ~875 K, whereas supported SnO_2 was reduced in a two-step process: from +4 to +2 at ~630 K and from +2 to 0 at ~900 K. The data acquired matched those found in the literature (Auroux *et al.*, 2000; Haneda *et al.*, 2001; Janiszewska *et al.*, 2009, Lazar *et al.*, 2000; Rodriguez *et al.*, 2005) in which a two-step reduction of SnO_2 supported on porous material (*i.e.* zeolites, various oxide supports) was reported. In the case of unmodified magadiite, a small broad peak with a maximum at ~600 K was noticed. It may represent baking of the bed.

For samples with lamellar Sn^{4+}, due to stabilization of the isolated Sn ions by the silica layer, one can expect a shift of the maximum temperature of the first step of reduction towards higher values. Such a shift, from ~630 K to ~700–720 K, can be observed in all Sn-magadiite synthesized. The second step's peak was noticed at ~870 K. The surfaces beneath the first and second steps of Sn^{4+} reduction were measured and found to be equal, confirming the two-step reduction process. An additional peak or shoulder in the lower-temperature region can be attributed to the reduction of non-bonded, well dispersed Sn on the external surface.

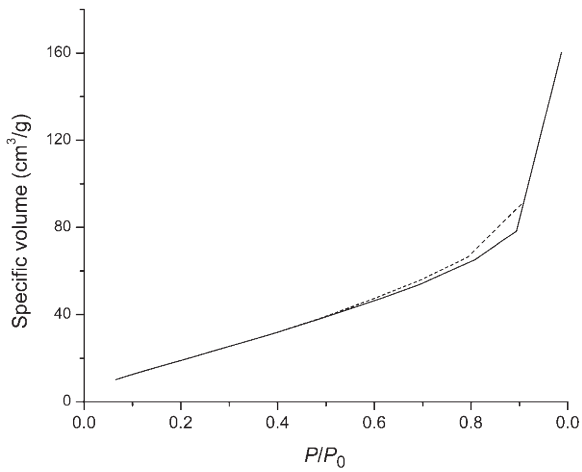

Figure 8. Adsorption isotherm of Na-magadiite synthesized in the presence of Na_2CO_3.

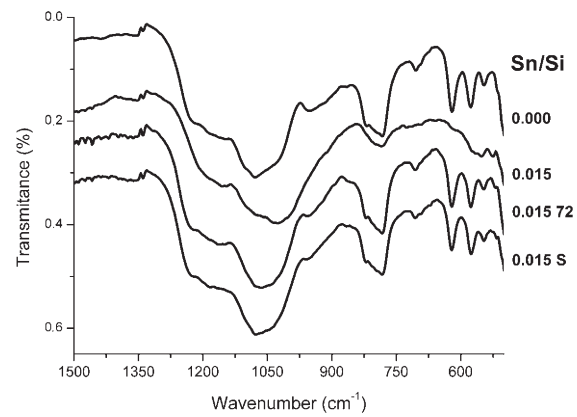

Figure 9. IR spectra of various Na forms of Sn-containing samples synthesized with Na_2CO_3. S: synthesis with magadiite seeds.

https://doi.org/10.1346/CCMN.2012.0600303 Published online by Cambridge University Press

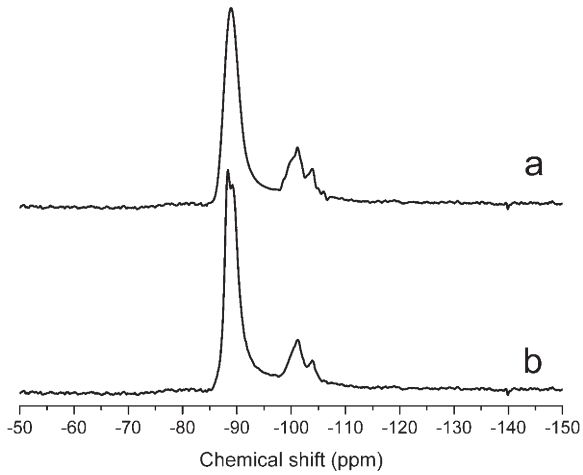

Figure 10. ^{29}Si MAS NMR spectra of (a) Na-magadiite and (b) 0.015 Sn magadiite synthesized in the presence of Na_2CO_3.

The acidity of the H forms of the synthesized samples was investigated by TPAD. The introduction of the heteroatom led to a shift in the temperature of NH_3 desorption (Figure 12). The lower temperature of NH_3 desorption for the Sn-magadiite, in comparison with the Na-magadiite, suggests that the presence of Sn reduced the acidity of the material. A slightly higher temperature of NH_3 desorption, for samples synthesized without Na_2CO_3, indicated the greater acidity of those samples. In the case of the Al samples, an additional desorption maximum (~ 770 K) was detected, indicating the presence of a bridged Al-OH-Si species, typical of crystalline aluminosilicates, probably due to the negative charge of AlO_4^- tetrahedra.

The nature of the active sites of the synthesized samples was investigated in the decomposition of 2-methyl-3-butyn-2-ol (MBOH). Depending on the type of active site, different products can be detected (Figure 13) (Lauron-Pernot *et al*., 1991).

The average conversion of MBOH for all samples in the Na form did not exceed 17% (Figure 14). Samples

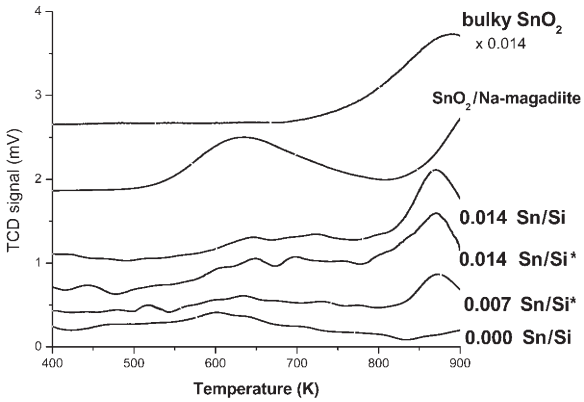

Figure 11. H_2-TPR profiles of various samples. * synthesis without Na_2CO_3.

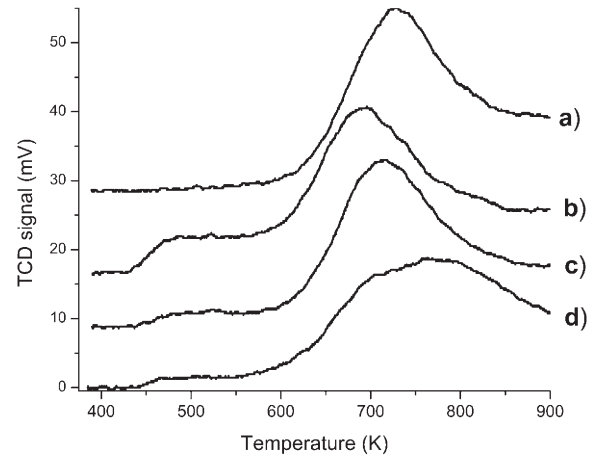

Figure 12. TPAD profiles of the H forms of various samples: (a) 0.000 Sn/Si synthesized with Na_2CO_3; (b) 0.015 Sn/Si synthesized with Na_2CO_3; (c) 0.015 Sn/Si synthesized without Na_2CO_3; (d) 0.003 Al/Si synthesized with Na_2CO_3.

synthesized without the presence of Na_2CO_3 exhibited a slightly lower conversion. Similar main products (acetone and acetylene) and similar selectivity were detected in the case of the Na forms of all unmodified and modified magadiite samples, indicating the almost exclusive presence of basic active sites (Figure 15).

A decrease in conversion, in comparison with Na forms, was observed for the H forms of all unmodified samples and Sn-magadiite (Figure 14). The presence of MBYNE, as well

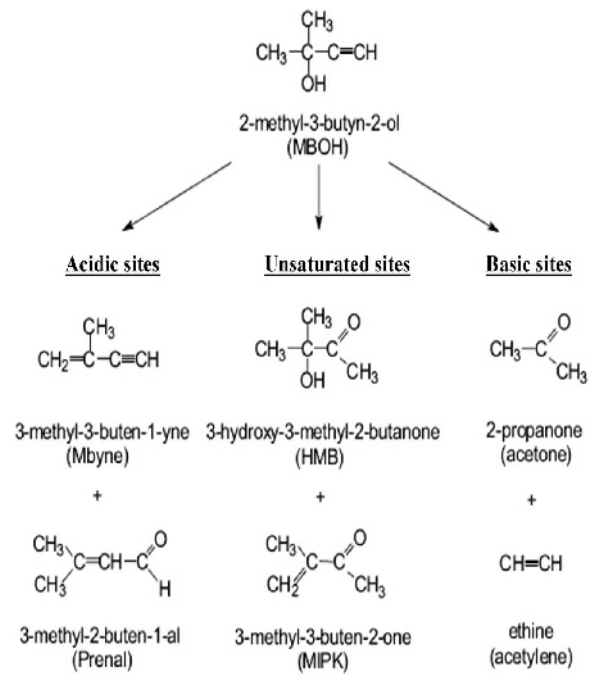

Figure 13. Possible products of MBOH reaction depending on the nature of the active sites.

https://doi.org/10.1346/CCMN.2012.0600303 Published online by Cambridge University Press

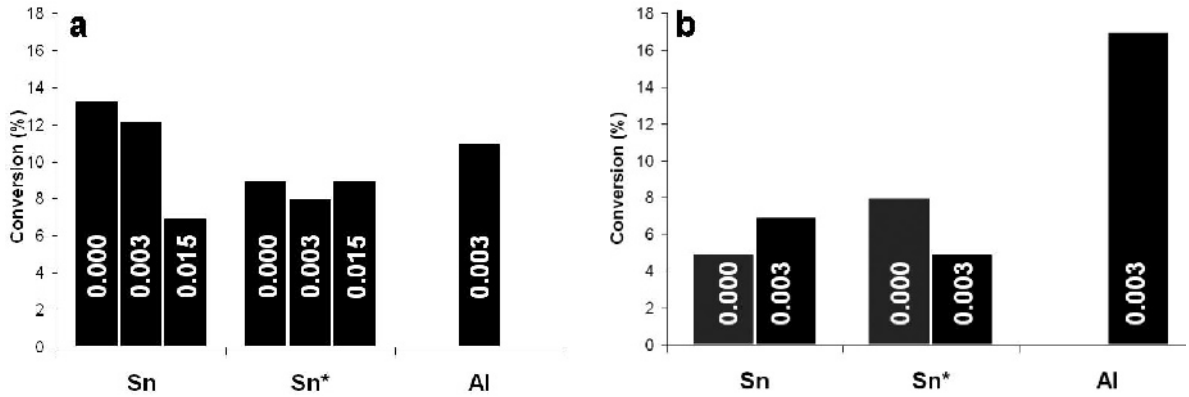

Figure 14. Conversion of MBOH over different samples after 66 min on stream. *M*/Si ratios are given in columns. * synthesis without Na_2CO_3. (a) Na forms, (b) H form.

as acetone and acetylene, suggests a heterogeneous character of the surface of the samples tested. No meaningful differences were found between Sn-containing and unmodified samples, indicating the absence of additional negative charges on the sample surface. On the other hand, no conversion changes were observed in the case of the H form of Al-containing samples. The presence of MBYNE as the main product (Figure 15) indicates an acidic character of the surface, generated by the presence of the negative charge from AlO_4^- tetrahedra. The results obtained correspond well with the TPAD data (Figure 12).

CONCLUSIONS

The Sn-containing magadiite structures were synthesized successfully with Sn/Si ratios up to 0.015. All magadiite samples exhibited the same distance between the layers. No conclusive evidence was found for the existence of pillars or impurities between the layers. The presence of Sn in the layers is not clearly reflected in IR spectra. Nevertheless, the split of the Q_3 signal in ^{29}Si MAS NMR spectra might indicate the presence of the Si-O-Sn species in the silicate layers.

The redox properties of the Sn-modified samples were proven by H_2-TPR. The amount of reduced Sn increased with increasing Sn content in the samples. Moreover, shifts in the temperature of the reduction steps may be confirmation of the presence of the SnO_4 tetrahedra incorporated into silica layers. The H_2-TPR profiles also confirmed the presence of moderate amounts of Sn species on the surfaces of the magadiite crystals.

The synthesis method for the Sn-modified magadiite was not suitable for the introduction of Al in amounts similar to those reported by other authors.

Unlike the morphology, the nature of the sample's active sites changed significantly after the introduction of the heteroatom. Due to the negative charge of AlO_4^- tetrahedra, H forms of the Al-containing samples resulted in stronger acid sites than did the unmodified magadiite, whereas the introduction of Sn led to the formation of weaker acid sites. No meaningful difference was detected between the selectivity of the Sn-containing and unmodified samples in MBOH reaction and thus Sn(IV) can be assumed to have been incorporated with coordination number 4. Samples

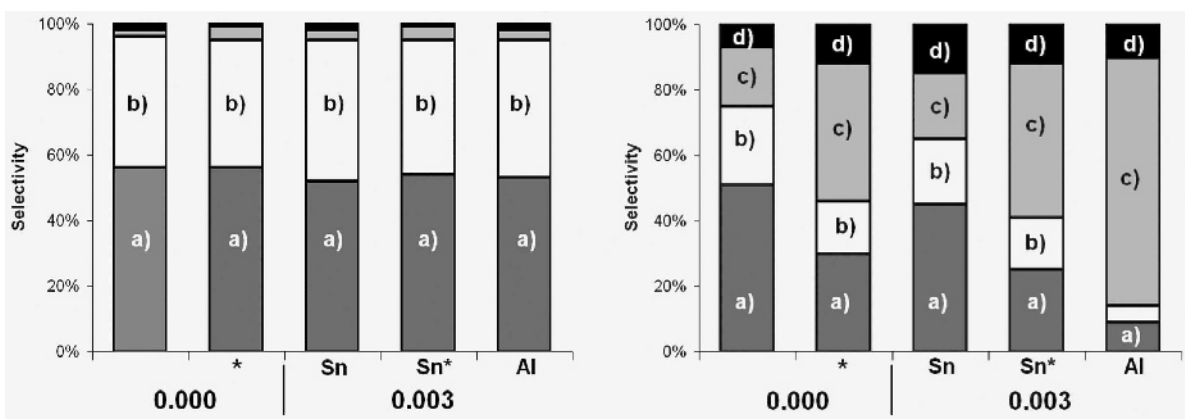

Figure 15. Selectivity toward: (a) acetone; (b) acetylene; (c) MBYNE; (d) others, over different samples after 66 min on stream. *M*/Si ratios are given under the charts. * synthesis without Na_2CO_3. (left) Na forms; (right) H form.

https://doi.org/10.1346/CCMN.2012.0600303 Published online by Cambridge University Press

synthesized without the presence of Na_2CO_3 exhibited slightly higher acidity.

ACKNOWLEDGMENTS

Wojciech Supronowicz gratefully acknowledges the German Academic Exchange Service (DAAD) for supplying a research grant. The authors thank CWK Bad Koestritz (Germany) for the donation of chemicals.

The authors thank J. Ofili (University Erlangen-Nuremberg) for an introduction to low-angle XRD and the discussion of these results.

REFERENCES

Almond, G.G., Harris, R.K., and Franklin, K.R. (1997) A structural consideration of kanemite, octosilicate, magadiite and kenyaite. *Journal of Materials Chemistry*, **7**, 681–687.

Auroux, A., Sprinceana, D., and Gersavini, A. (2000) Support effects on de-NOx catalytic properties of supported tin oxides. *Journal of Catalysis*, **195**, 140–150.

Azizi, S.N. and Yousefpour, M. (2011) Isomorphous substitution of iron and nickel into analcime zeolite. *Zeitschrift für anorganische und allgemeine Chemie*, **637**, 759–765

Borbely, G., Beyer, H.K., Karge, H.G., Schwieger, W., Brandt, A., and Bergk, K.H. (1991) Chemical characterization, structural features, and thermal behavior of sodium and hydrogen octosilicate. *Clays and Clay Minerals*, **39**, 490–497.

Boronat, M., Concepcion, P., Corma, A., and Renz, M. (2007) Peculiarities of Sn-Beta and potential industrial applications. *Catalysis Today*, **121**, 39–44.

Brindley, G.W. (1969) Unit cell of magadiite in air, in vacuo, and under other conditions. *American Mineralogist*, **54**, 1583–1591.

Camblor, M.A., Corma, A., and Perez-Pariente, J. (1993) Infrared spectroscopic investigation of titanium in zeolites. A new assignment of the 960 cm^{-1} band. *Journal of the Chemical Society, Chemical Communications.* **6**, 557–559.

Corma, A., Domine, M.E., and Valencia, S. (2003) Water-resistant solid Lewis acid catalysts: Meerwein-Ponndorf-Verley and Oppenauer reactions catalyzed by tin-beta zeolite. *Journal of Catalysis*, **215**, 294–304.

Feng, F. and Balkus Jr., K.J. (2003) Synthesis of kenyaite, magadiite and octosilicate using poly(ethylene glycol) as a template. *Journal of Porous Materials*, **10**, 5–15.

Feng, F. and Balkus Jr., K.J. (2004) Recrystallization of layered silicates to silicalite – 1. *Microporous and Mesoporous Materials*, **69**, 85–96.

Fletcher, R.A. and Bibby, D.M. (1987) Synthesis of kenyaite and magadiite in the presence of various anions. *Clays and Clay Minerals*, **35**, 318–320.

Fudala, Á., Kónya, Z., Kiyozumi, Y., Niwa, S.-I., Mizukami, F., Lentz, P.B., Nagy, J., and Kiricsi, I. (2000) Preparation, characterization and application of the magadiite based mesoporous composite material of catalytic interest. *Microporous and Mesoporous Materials*, **35–36**, 631–641.

Haneda, M., Ohzu, S., Kintaichi, Y., Shimizu, K., Shibata, J., Yoshida, H., and Hamada, H. (2001) Sol-gel prepared Sn-Al_2O_3 catalysts for the selective reduction of NO with propene. *Bulletin of the Chemical Society of Japan*, **74**, 2075–2081.

Iwasaki, T., Kuroda, T., Ichio, S., Satoh, M., and Fujita, T. (2006) Seeding effect on crystal growth in hydrothermal synthesis of layered octosilicate. *Chemical Engineering Communications*, **193**, 69–76.

Janiszewska, E., Kowalak, S., Supronowicz, W., and Roessner, F. (2009) Synthesis and properties of stannosilicates. *Microporous and Mesoporous Materials*, **117**, 423–430.

Khouw, C.B. and Davis, M.E. (1995) Catalytic activity of titanium silicates synthesized in the presence of alkali-metal and alkaline-earth ions. *Journal of Catalysis*, **151**, 77–86.

Kim, M.H., Ko, Y., Kim, S.J., and Uh, Y.S. (2001) Vapor phase Beckmann rearrangement of cyclohexanone oxime over metal pillared ilerite. *Applied Catalysis A*, **210**, 345–353.

Kim, S.J., Jung, K.-D., Joo, O.-S., Kim, E.J., and Kang, T.B. (2004) Catalytic performance of metal oxide-loaded Ta-ilerite for vapor phase Beckmann rearrangement of cyclohexanone oxime. *Applied Catalysis A*, **266**, 173–180.

Kiyozumi, Y., Salou, M., Mizukami, F., Nair, P., Maeda, K., and Niwa, S. (1998) Influence of solid-state transformation time on the nucleation and growth of silicalite 1 prepared from layered silicate. *Journal of Materials Chemistry*, **8**, 2125–2132.

Kiyozumi, Y., Salou, M., and Mizukami, F. (2002) Synthesis of hybrid zeolite disc from layered silicate. *Studies in Surface Science and Catalysis*, **142A**, 231–238.

Kuhlmann, A., Roessner, F., Schwieger, W., and Gravenhorst, O. (2004) New bifunctional catalyst based on Pt containing layered silicate Na-ilerite. *Catalysis Today*, **97**, 303–306.

Lagaly, G., Beneke, K., and Weiss, A. (1975) Magadiite and H-magadiite: II. H-magadiite and its intercalation compounds. *American Mineralogist*, **60**, 650–658.

Lauron-Pernot, H., Luck, F., and Popa, J.M. (1991) Methylbutynol: a new and simple diagnostic tool for acidic and basic sites of solids. *Applied Catalysis*, **78**, 213–225.

Lazar, K., Chandwadkar, A.J., Fejes, P., Cejka, J., and Ramaswamy, A.V. (2000) Valency changes of iron and tin in framework-substituted molecular sieves investigated by *in situ* Mössbauer spectroscopy. *Journal of Radioanalytical and Nuclear Chemistry*, **246**, 143–148.

Li, B., Li, X., Xu, J., Pang, X., Gao, X., and Zhou, Z. (2010) Synthesis and characterization of composite molecular sieves M_1-MFI/M_2-MCM-41(M_1, M_2 = Ni, Co) with high heteroatom content and their catalytic properties for hydrocracking of residual oil. *Journal of Colloid and Interface Science*, **346**, 199–207.

Macedo, T.R. and Airoldi, C. (2006) Host lamellar silicic acid magadiite for some heterocyclic amine inclusions and quantitative calorimetric data. *Microporous and Mesoporous Materials*, **94**, 81–88.

Mihályi, R.M., Pál-Borbély, G., Beyer, H.K., Szegedi, Á., and Korányi, T.I. (2007) Characterization of aluminum and boron containing beta zeolites prepared by solid-state recrystallization of magadiite. *Microporous and Mesoporous Materials*, **98**, 132–142.

Ozawa, K., Iso, F., Nakao, Y., Cheng, Z., Fujii, H., and Yamaguchi, H.J. (2007) Preparation and characterization of Ag-magadiite nanocomposites. *Journal of the European Ceramic Society*, **27**, 2665–2669.

Pál-Borbély, G., Beyer, H.K., Kiyozumi, Y., and Mizukami, F. (1997) Recrystallization of magadiite varieties isomorphically substituted with aluminum to MFI and MEL zeolite. *Microporous and Mesoporous Materials*, **11**, 45–51.

Pál-Borbély, G., Beyer, H.K., Kiyozumi, Y., and Mizukami, F. (1998) Synthesis and characterization of a ferrierite made by recrystallization of an aluminium-containing hydrated magadiite. *Microporous and Mesoporous Materials*, **22**, 57–68.

Peng, S., Gao, Q., Du, Z., and Shi, J. (2006) Precursors of TAA-magadiite nanocomposites. *Applied Clay Science*, **31**, 229–237.

Renz, M., Blasco, T., Corma, A., Fornes, V., Jensen, R., and Nemeth, L. (2002) Selective and shape-selective Baeyer–Villiger oxidations of aromatic aldehydes and cyclic ketones with Sn-Beta zeolites and H_2O_2. *Chemistry – A European Journal*, **8**, 4708–4717.

Rodriguez, R., Pfaff, C., Melo, L., and Betancourt, P. (2005) Characterization and catalytic performance of a bimetallic

Pt-Sn/HZSM-5 catalyst used in denitratation of drinking water. *Catalysis Today*, **107**–**108**, 100–105.

Royer, B., Cardoso, N.F., Lima, E.C., Macedo, T.R., and Airoldi, C. (2010) A useful organofunctionalized layered silicate for textile dye removal. *Journal of Hazardous Materials*, **15**, 366–374.

Schwieger, W., Gravenhorst, O., Selvam, T., Roessner, F., Schloegl, R., Su, D., and Mabande, G.T.P. (2003) Preparation of highly loaded platinum nanoparticles on silica by intercalation of $[Pt(NH_3)_4]^{2+}$ ions into layered sodium silicate ilerite. *Colloid and Polymer Science*, **281**, 584–588.

Selvam, T., Bandarapu, B., Mabande, G.T.P., Toufar, H., and Schwieger, W. (2003) Hydrothermal transformation of a layered sodium silicate, kanemite, into zeolite Beta (BEA). *Microporous and Mesoporous Materials*, **64**, 41–50.

Szostak, R., Nair, V., and Thomas, T.L.J. (1987) Incorporation and stability of iron in molecular-sieve structures. Ferrisilicate analogues of zeolite ZSM-5. *Journal of the Chemical Society, Faraday Transactions 1*, **83**, 487–495.

Sprung, R., Davis, M.E., Kauffman, J.S., and Dybowski, C. (1990) Pillaring of magadiite with silicate species. *Industrial and Engineering Chemistry Research*, **29**, 213–220.

Superti, G.B., Oliveira, E.C., Pastore, H.O., Bordo, A., Bisio, C., and Marchese, L. (2007) Aluminum magadiite: an acid solid layered material. *Chemistry of Materials*, **19**, 4300–4315.

Supronowicz, W. and Roessner, F. (2011) Influence of Sn and Al heteroatoms on the synthesis of ilerite. *Clays and Clay Minerals*, **59**, 95–105.

Wang, Y.-R., Wang, S.-F., and Chang, L.-C. (2006) Hydrothermal synthesis of magadiite. *Applied Clay Science*, **33**, 73–77.

Wang, S.-F., Lin, M.-L., Shieh, Y.-N., Wang, Y.-R., and Wang, S.-J. (2007) Organic modification of synthesized clay-magadiite. *Ceramics International*, **33**, 681–685.

Yanagisawa, T., Shimizu, T., and Kuroda, K.C. (1990) Trimethylsilyl derivatives of alkyltrimethylammonium–kanemite complexes and their conversion to microporous SiO_2 materials. *Bulletin of the Chemical Society of Japan*, **63**, 1535–1537.

Yu, J. and Yang, Q-.Y. (2010) Magnetization improvement of Fe-pillared clay with application of polyetheramine. *Applied Clay Science*, 48, 185–190.

(*Received 13 October 2011; revised 23 February 2012; Ms. 628; A.E. S.M. Kuznicki*)